International Forum on Aeroelasticity and Structural Dynamics
IFASD 2017
25–28 June 2017, Como - Italia

THE AEROELASTIC BEHAVIOUR OF A FORWARD-SWEPT WING CONFIGURATION WITH FOCUS ON ENGINE GYROSCOPICS AND T-TAIL FLUTTER

Stefan Waitz [1]

[1] DLR — German Aerospace Center
Institute of Aeroelasticity
Bunsenstr. 10, 37073 Göttingen, Germany
stefan.waitz@dlr.de

Keywords: forward sweep, T-tail flutter, gyroscopics, engine thrust, follower force, asymmetric eigenmode, engine aeroelasticity, critical speed, flutter frequency, laminar flow

Abstract

Since more and more modern civil aircraft for reasons of fuel efficiency and environmental aspects are equipped with UHBR-engines, the need to tackle specific engine related dynamic problems has occured. The request for UHBR-engines with high bypass ratio numbers and with their intrinsic advantages of economic fuel consumption and lower acoustic emission asks for enhanced prediction capabilities. Beside the energetic benefits such engines add to the aircraft design their rotating large diameter fans can influence the dynamic behaviour of the complete elastic aircraft fuselage in a very unfavourable manner. Especially in the scenario when large rotating engine masses are to be combined with elastic suspension structures the possible occurance of structural vibration problems can be avoided by taking the gyroscopic effects into account. As another important engine related question the modelling and the impact of the engine thrust is highlighted by integration of the follower force induced terms into the dynamical simulation model.

A further approach towards lower fuel consumption is the drag reduction of the airplane. This can be realized by keeping the flow field around the wing surfaces laminar as much as possible. With the ALLEGRA-S configuration a short and medium range aircraft has been designed with the aim of drag reduction by keeping the wing flow laminar as long as possible. Together with laminar aerodynamic wing airfoil sections the forward sweep of the wings has a favourable influence on the laminar character of the wing flow. The forward swept wings as well as the T-tail empennage and the backward position of the engine nacelles on both sides of the fuselage also have a formative influence on the flutter behaviour and thus the stability margings of the design. The flutter behaviour of several baseline mass configurations has been examined. Important questions with regard to the enhancement of the flutter model and the impact on structural dynamics and aeroelasticity are treated in this work. For example by introducing additional d.o.f. coupling into the aeroelastic model the component correction terms have influenced particular flutter eigenmodes and caused (minor) deviations in flutter frequencies and velocities.

1 INTRODUCTION

Fuel efficiency of civil aircraft is a major goal in the design of modern civil air vehicles where both economic and environmental aspects are involved. A fundamental approach towards lower fuel consumption is the drag reduction of the airplane. One way this goal can be realized is keeping the flow field around the fuselage and the wing surfaces laminar as long as possible thus reducing the viscous drag. In the DLR projects IGREEN and ALLEGRA questions around a modern laminar aircraft design were treated. With the ALLEGRA-S configuration a short and medium range aircraft has been designed with the aim of drag reduction by keeping the wing flow laminar over wide areas of the wing surface (see Fig. 1). After several foregoing design phases the ALLEGRA-S design is the first overall composite structural design. Together with laminar aerodynamic wing profiles the forward sweep of the wings has a favourable influence on the laminar character of the wing flow. Two further advantages of this specific design can be named: The forward swept wings stabilize the flow around the ailerons against flow separation thus lowering the risk of loss of the transverse controllability. And also the passenger comfort is increased by the positive dynamic behaviour of the aircraft structure towards gust response. A drawback of the forward swept wings in comparison to the conventional design of aircraft with backward sweep lies in an elevated risk towards static divergence instability. Like more and more modern civil aircraft for reasons of fuel efficiency and environmental aspects the examined design is equipped with UHBR engines which result in the need to tackle specific engine related dynamic problems in addition. The request for UHBR engines with high bypass ratio numbers and with their intrinsic advantages of economic fuel consumption and lower acoustic emission asks for enhanced prediction capabilities w.r.t. rotor dynamics.

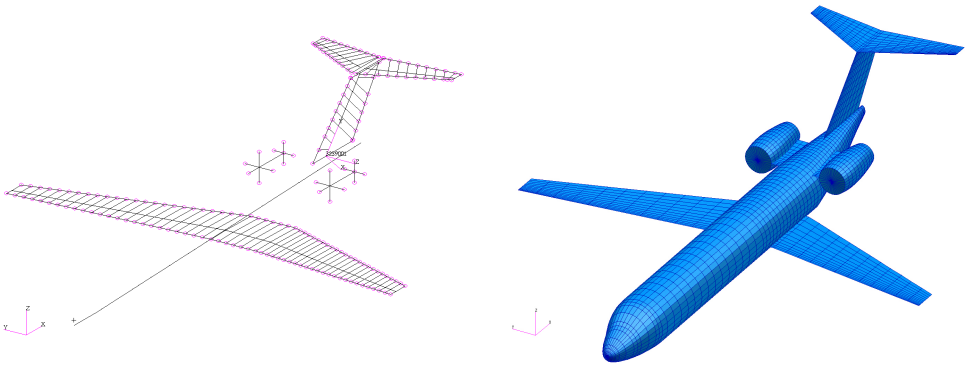

Figure 1: The structural FE model and the aerodynamic panel model of ALLEGRA-S

The objective of this study is the investigation of the dynamic aeroelastic stability of the ALLEGRA-S forward swept aircraft design. With numerical aeroelastic simulations for several mass configurations and flight levels the flutter behaviour was examined. With the examination of the critical flight speed not only the lowest flutter case has been determined numerically but also the higher flutter cases have been studied with a look on the nature of possible other modes of flutter which could become relevant for example in case of the extinction of lower flutter modes. The occuring flutter modes of the examined mass configurations could systematically be sorted in three groups of qualitatively similar flutter modes.

Special questions with regard to structural dynamics and aeroelasticity were incorporated into the flutter analyses treated in this work. Beside the energetic benefits the UHBR engines add to the aircraft design their rotating large diameter fans can influence the dynamic behaviour of the complete elastic aircraft fuselage in a very unfavourable manner. Especially in the scenario when large rotating engine masses are to be combined with elastic suspension structures the possible occurance of structural vibration problems can be avoided by taking the gyroscopic effects into account. As another important engine related question the modelling and the impact of the engine thrust is highlighted by integration of the follower force induced terms into the dynamical simulation model. In terms of an undisturbed wing flow furthermore the two engine nacelles are positioned at the rear part of the fuselage and the horizontal stabilizer is positioned at the upper end of the vertical tail plane (VTP) in a so called T-tail configuration. The forward swept wings as well as the T-tail empennage and the backward position of the engines have a formative influence on the flutter behaviour and thus the stability margins of the design.

2 INVESTIGATED AIRPLANE MODEL BUILD-UP

In the frame of the DLR project ALLEGRA the forward swept wing configuration ALLEGRA-S has been submitted to a dynamic aeroelastic analysis. Objective for the flutter calculations had been a structural Finite Element model which had been elaborated as part of the project with the FE code NASTRAN. The description of the aerodynamic model required for the unsteady aeroelastic simulation was formulated in the Doublet Lattice code ZAERO. A DLM grid had been built up for the discretization of the unsteady surface pressure distribution on the fuselage, empennage and the wings (see Fig. 1).

	Mass configuration c01	Mass configuration c09
Mass case	MFW	MTOW
Mass [kg]	43712	73365
Fuel mass [kg] / [%]	0 / 0	16.980 / 100
Cg position [m]	19.637	20.239
Wing span [m]	35.8	35.8
Wing area [m^2]	132.0	132.0
Wing sweep 25%c [^{o}]	-19.8	-19.8
Wing sweep LE [^{o}]	-17.0	-17.0
NASTRAN solver	SOL 103	SOL 103
FE nodes (condens.)	400	400
Aerodynamic boxes	3828	3828
Number eigenmodes	86	86

Table 1: Design parameters of the ALLEGRA-S mass configurations c01 and c09 for the basic flutter simulations

The engine nacelles had been modelled both structurally (as rigid body) and aerodynamically with surface panels and with body elements (the latter have been used for the presented results). Together with a set of elastic eigenmodes of the aircraft structure and the self induced unsteady aerodynamic forces caused by the perturbation velocities an equation of motion in reduced modal coordinates was built up. This homogeneous equation had

been evaluated by a subsequent eigenvalue solution for stability behaviour. The structural modal basis had been calculated with NASTRAN before being imported into ZAERO where the aerodynamic (plus eventual correction) terms had been added and solved in the linear aeroelastic stability analysis. Some basic model data can be found in Tab. 1, additional in Tab. 8. The flutter calculations were executed with six rigid body modes plus the first 80 elastic eigenmodes serving as generalized modal d.o.f. Some of the lower structural eigen frequencies are listed in Tab. 2.

The structural part of the aeroplane was built up by a FEM stick model where fuselage, wings and empennage were composed by about 100 beam elements (see Fig. 1 and Tab. 1) as condensed from the original high resolution FE model, with approximately 600 reduced degrees of freedom comprising the A-set of the solver. Within the commercial code NASTRAN (SOL 103) the eigenvalue solution of the discretized linear equations of motion rendered the necessary set of eigenfrequencies and eigenshapes. Out of this set the first 86 modes, including the six zero frequency rigid body motion shapes (see Tab. 2), had been extracted and imported into the flutter solver for further use. The commercial code ZAERO then had been applied for both the build-up of the aerodynamic part of the aeroplane model and the solving of the complete aeroelastic equation of motion in the frequency domain. The aerodynamic model (see Fig. 1) was composed of roughly 2200 DLM wing and body panels (boxes). Together with the structural eigenmodes interpolated onto the aerodynamic grid the final equation system was assembled. After a modal transformation by the 86 vacuum modes it was reduced to just this respective number of modal d.o.f.

	c01	c09		c01	c09		c01	c09
7	3.3200	2.3914	27	19.896	13.448	47	41.458	25.886
8	3.3844	3.1587	28	20.009	13.711	48	43.306	25.917
9	3.9882	3.7381	29	20.268	13.719	49	43.573	26.144
10	4.7360	4.1070	30	21.356	14.486	50	43.864	26.889
11	4.9078	4.3059	31	22.294	15.371	51	45.198	27.270
12	5.3126	4.3989	32	22.652	16.169	52	45.535	28.427
13	5.8683	5.2393	33	23.048	16.671	53	45.668	29.547
14	6.9919	5.8151	34	25.187	17.309	54	46.761	29.861
15	7.3259	5.9087	35	26.153	17.624	55	46.886	30.608
16	7.5869	6.5625	36	26.268	18.096	56	47.645	30.839
17	7.7050	7.3434	37	26.722	18.561	57	47.894	31.542
18	9.0996	7.3926	38	28.991	20.020	58	52.101	31.948
19	9.5219	8.3609	39	29.068	20.061	59	54.485	34.024
20	10.157	8.9850	40	30.655	21.358	60	54.604	34.948
21	12.575	9.1784	41	30.898	21.383	61	55.082	35.381
22	14.597	9.3288	42	32.144	21.519	62	55.694	35.903
23	15.390	10.289	43	33.325	22.567	63	58.482	36.230
24	16.986	10.343	44	37.103	22.757	64	59.057	37.419
25	17.010	12.310	45	39.662	23.877	65	59.181	37.572
26	18.562	12.807	46	40.334	25.473	66	59.715	38.318

Table 2: The 60 lower elastic eigenfrequencies of the ALLEGRA-S mass configurations c01 and c09

3 FLUTTER BEHAVIOUR OF THE BASELINE CASES

As a first step the baseline configuration had been investigated. In this case the engines were taken into account as if being in a non-rotating state, i.e. they contributed to the aeroelastic aircraft model "only" with their engine masses and rotational inertias in a rigid body sense and, being elastically mounted, they established the respective d.o.f. Since the structure of the aeroplane is (almost) symmetric, the solution of the aeroelastic eigenvalue problem renders only eigenmodes which are either symmetric or antimetric w.r.t. the vertical center plane. Therefore in the case of the occurrence of flutter instabilities the corresponding flutter modes also show either symmetric or antimetric properties. The results of the eigenvalue formulation are presented on one hand as a set of the complex eigenvalues as a function of the flight speed (frequencies and damping/excitation) and on the other hand as the corresponding complex eigenmodes (see Fig. 6 to Fig. 8). The eigenvalue results are used to build up the flutter curves (see Fig. 2 to Fig. 5 and Fig. 9).

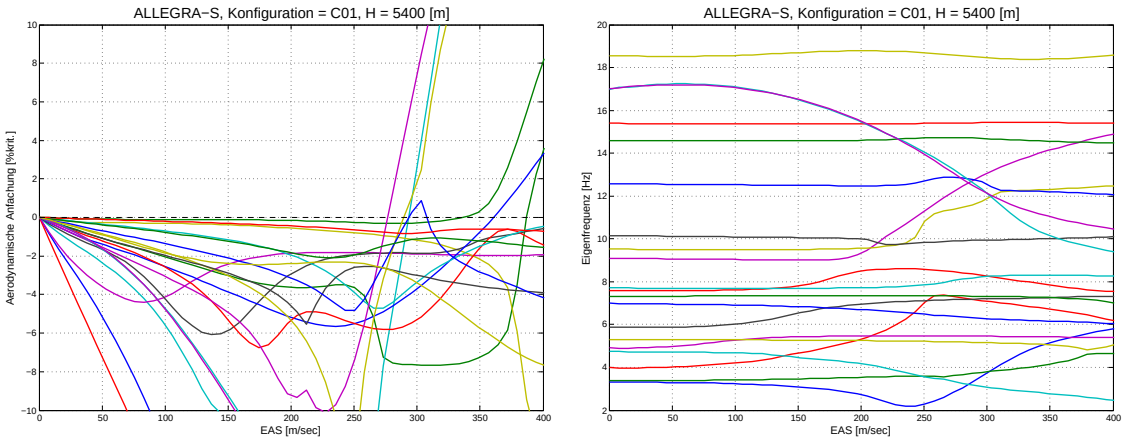

Figure 2: *Aerodynamic excitation* and *frequencies* of the first 20 elastic eigenmodes, ALLEGRA-S, configuration c01, ISA 15°C, H = 5400 [m]

Flutter case No.	eigenmode No.	Frequency f [Hz]	EAS [m/sec]	TAS [m/sec]	Flutter type
1	8	f = 4.6378	386.63	509.73	T-tail (fuselage-bend)
2	10	f = 3.1210	293.30	386.68	T-tail (fuselage-roll)
3	14	f = 6.1403	360.44	475.20	Wing-ant (vert, + Eng)
4	15	f = 7.2880	337.11	444.44	Wing-sym (hori)
5	18	f = 12.3209	276.56	364.61	HTP-sym
6	19	f = 11.6098	289.39	381.53	HTP-ant
7	21	f = 12.7075	293.62	387.11	HTP-ant

Table 3: Classification of *flutter modes*, ALLEGRA-S, configuration c01 (43,71 [t]), ISA 15°C, H = 5400 [m]; compare Fig. 6

In the flutter curves which are displaying damping and frequencies w.r.t. the flight speed (see for example Fig. 2) the distinct flutter cases are to be detected by the sign change of the

real part of the eigenvalues from negative to positive, here displayed as negative aerodynamic damping (= aerodynamic excitation), since there was no material damping allocated in the structure. Within the group of flutter cases (see Tab. 3) we can perceive two instable modes which are shaped by a considerable movement of the empennage due to the T-tail of this aircraft design. These instability cases (flutter case 1 and 2) occur both antimetric, while the lower one goes along with a predominant wing heave (for the mode shapes see Fig. 6). Prior to these two flutter cases there occur other 3 flutter states at the critical flight speed of around 280 [m/sec] EAS. These lowest flutter cases are of symmetric or antimetric nature with only moderate wing deflections and mainly driven by a vertical HTP motion. Since their excitation ratios are rising with a steep slope they have to be considered more dangerous than those which are rising only moderately with the flight speed. Because such flutter cases often reach only small values ($< .5[\%]$) we can ignore them in our investigation.

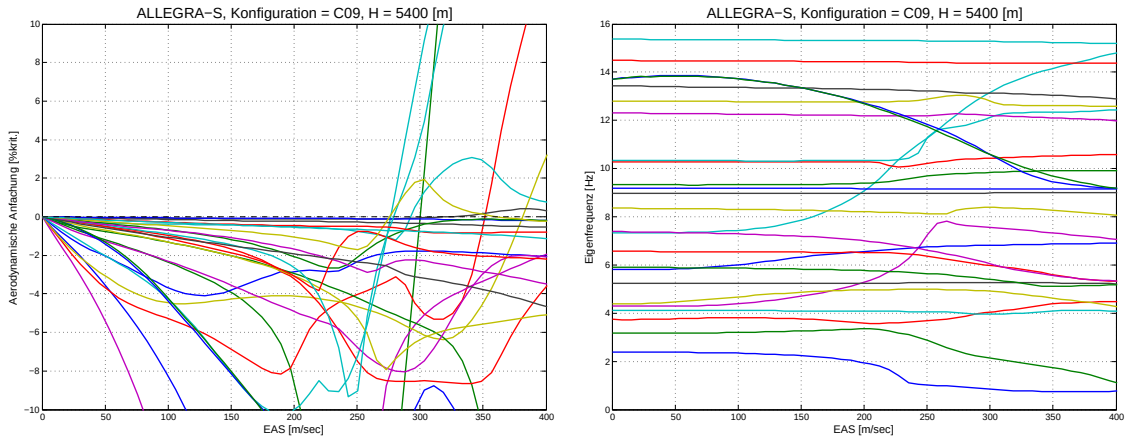

Figure 3: *Aerodynamic excitation* and *frequencies* of the first 25 elastic eigenmodes, ALLEGRA-S, configuration c09, ISA 15°C, H = 5400 [m]

Flutter case No.	eigenmode No.	Frequency f [Hz]	EAS [m/sec]	TAS [m/sec]	Flutter type
1	8	f = 2.1282	300.11	395.67	Wing-ant (vert)
2	9	f = 4.3915	351.55	463.48	T-tail (fuselage-bend)
3	10	f = 3.9517	292.48	385.60	T-tail (fuselage-bend)
4	12	f = 4.4276	381.18	502.55	Wing-sym (vert)
5	13	f = 5.2546	321.94	424.45	Wing-sym (hori)
6	17	f = 12.3726	276.59	364.65	HTP-sym
7	24	f = 11.7860	278.89	367.69	HTP-ant
8	26	f = 13.0382	275.85	363.68	HTP-ant

Table 4: Classification of *flutter modes*, ALLEGRA-S, configuration c09 (73,36 [t]), ISA 15°C, H = 5400 [m]

All aeroelastic simulations presented in this paper were conducted under ISA atmospheric conditions at sea level or at 5400 [m] and 11000[m] flight level. The results of the flutter calculations were produced in a non-matched point analysis with the Ma number set

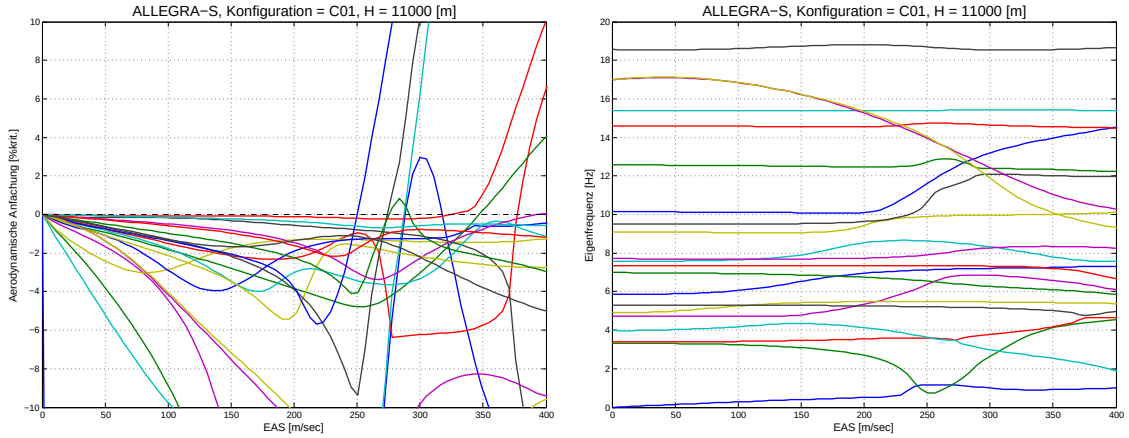

Figure 4: *Aerodynamic excitation* and *frequencies* of the first 21 elastic eigenmodes, ALLEGRA-S, configuration c01, ISA 15°C, H = 11000 [m]

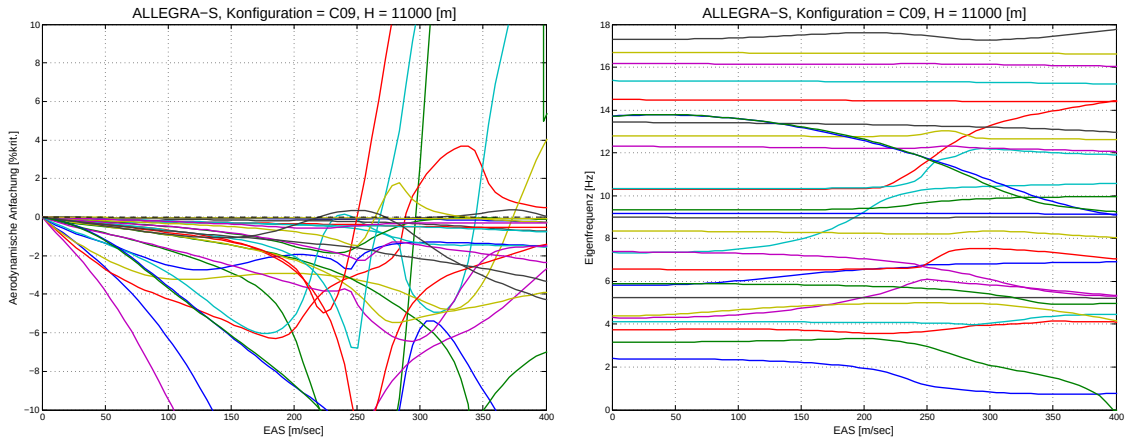

Figure 5: *Aerodynamic excitation* and *frequencies* of the first 28 elastic eigenmodes, ALLEGRA-S, configuration c09, ISA 15°C, H = 11000 [m]

to the value Ma = 0.80 (= 0.75 in Tab. 7). A higher converged Ma number was considered to be negligible, especially for the assessment of relative differences in the flutter results. The basic aeroelastic stability behaviour was investigated with two mass configurations. They consisted of the empty, light configuration "c01" and the heavy, fully loaded configuration "c09". For the cg position and the mass values see Tab. 1 and Tab. 8. The flutter analyses have been conducted for the two flight altitudes 5400 [m] und 11000 [m] with the ISA air densities of $\rho = 0,70478$ [kg/m^3] and $\rho = 0,363916$ [kg/m^3]. These two mass configurations and flight levels have been considered as most representative for the designed flight envelope. Although the identified flutter states were determined in *non-matched point* analyses the Mach number of the solutions fitted to the (lower) transsonic flight velocities. By setting the Mach number in the flutter calculations Ma = 0.8 the (linear) influence of the compressibility is captured but not the non-linear (and viscous) effects like compression shocks. As essential flutter analyses results the aerodynamic excitation (= negative damping) and the eigenfrequencies of the aeroelastic system are displayed in the flutter curves (see Fig. 2

to Fig. 5 and Fig. 9). In the diagrams the unstable (critical) states are defined by passing the flight velocity abscissa of the excitation curve from the negative into the positive area. In case of the flutter shapes as complex eigenmodes they here can be presented only as (better: animated) snapshots (Fig. 6 to Fig. 8). The flutter frequencies with the associated (critical) flight speeds as characteristic numbers of the flutter states are shown in Tab. 3 and Tab. 4 for flight altitude 5400 [m] and mass configurations "c01" and "c09". In the flutter curves (see Fig. 2 and Fig. 3) the corresponding branches of the frequencies and aerodynamic excitation can be found.

Although the lowest flutter case as the "critical" one is defining the dynamic stability behaviour of the aircraft design, it is worth looking also at the higher modes since they can reveal characteristic dynamic features which could become relevant in case of eventual design parameter changes. Looking at the found flutter states in this sense, the corresponding modes can be grouped in three "families", named as "flutter type" in the right columns of Tab. 3 and Tab. 4, but also Tab. 6, Tab. 7 and Tab. 9:

1. Those states denoted as "HTP" where the flutter modes as elastic deformations of the horizontal tail plane are predominantely local modes of the empennage. These states occur both anti- and symmetrical and are the cases with the lowest flutter speed (critical speed).

2. The flutter cases at the next higher speeds are global modes denominated "T-tail" where the VTP experiences a strong lateral elastical deformation while the HTP follows in a more or less rigid body movement. These only antimetric occuring modes are the characteristic T-tail shapes with the fuselage taken part in a rolling or lateral bending mode.

3. Finally the flutter modes denoted with "Wing" are the "classical" shapes where the empennage is still elastically deformed but plays no longer a dominant role. These states occur in an anti- and symmetric shape. As an unusual mode a symmetric flutter form with a strong horizontal fwd-aft motion with a coupled torsional content can be found in this group; this latter case appears only moderate excited for the mass configuration "c09" but the excitation can rapidly rise as for the mass configuration "c01" (see flutter mode 4 in Tab. 3 and Fig. 6 and mode 5 in Tab. 4).

The flutter speed values in Tab. 3 and Tab. 4 indicate how the predominant local shapes "HTP" are first to become instable. The flutter cases of the other flutter types lie in higher flight speed regions. The values of the instability velocities (as EAS values of the equivalent air speed) have in common that they get lowered by rising Ma numbers and flight altitudes but show clear variations related to the respective mass configuration. Two specific features of the T-tail dominated flutter cases have to be emphasised. They can be traced in the two T-tail flutter modes for example by comparison of the modal participation factors of mode 4 (rigid body roll), mode 8 (VTP torsion/bending) and mode 25 (antimetric wing torsion) in Tab. 5. The "T-tail" modes can be distinguished by the way how the fuselage is participating in the flutter mode which best can be studied in the "c01" mass configuration: In some of the T-tail flutter cases the fuselage has been subjected to a clear lateral elastic bending whereas in the other cases the fuselage participation consists of a rigid body roll, in both cases with the wings antimetrically bended (see flutter case 1 and 2 (mode 8 and 10) in Tab. 3 and Fig. 6). Another characteristic feature is the pronounced vertical plunging of the engine nacelles whilst counteracting the longitudinal fuselage rotation (denoted by "+Eng", like the 6.1403-Hz eigenmode in Tab. 3).

Together with the two major flutter parameters flutter speed and frequency the underly-

FLUTTER MODE TRACKING: 100% = PRIMARY MODE. 0% = NO CONTRIBUTION TO FLUTTER MODE.											
MODE(1) =	0.0000%,	MODE(2) =	1.9922%,	MODE(3) =	0.0006%,	MODE(4) =	11.4619%,	MODE(5) =	0.0071%,
MODE(6) =	6.4916%,	MODE(7) =	0.0066%,	MODE(8) =	100.0000%,	MODE(9) =	49.6209%,	MODE(10) =	39.4445%,
MODE(11) =	0.0040%,	MODE(12) =	28.3880%,	MODE(13) =	0.0002%,	MODE(14) =	9.5224%,	MODE(15) =	0.0002%,
MODE(16) =	0.0008%,	MODE(17) =	31.3227%,	MODE(18) =	0.0172%,	MODE(19) =	64.2562%,	MODE(20) =	0.0157%,
MODE(21) =	5.1511%,	MODE(22) =	2.2036%,	MODE(23) =	0.0001%,	MODE(24) =	0.0019%,	MODE(25) =	20.3362%,
MODE(26) =	0.0006%,	MODE(27) =	1.1850%,	MODE(28) =	0.0004%,	MODE(29) =	0.1269%,	MODE(30) =	6.8177%,
MODE(31) =	0.0003%,	MODE(32) =	0.0005%,	MODE(33) =	0.0234%,	MODE(34) =	0.0000%,	MODE(35) =	0.4025%,
MODE(36) =	0.0005%,	MODE(37) =	0.2457%,	MODE(38) =	0.0001%,	MODE(39) =	1.5045%,	MODE(40) =	0.0002%,
MODE(41) =	2.0958%,	MODE(42) =	0.0001%,	MODE(43) =	0.0092%,	MODE(44) =	3.6938%,	MODE(45) =	0.0005%,
MODE(46) =	0.2020%,	MODE(47) =	0.0000%,	MODE(48) =	0.0001%,	MODE(49) =	0.4805%,	MODE(50) =	2.1694%,
MODE(51) =	0.4825%,	MODE(52) =	0.0003%,	MODE(53) =	0.3264%,	MODE(54) =	0.0009%,	MODE(55) =	0.4537%,
MODE(56) =	0.0070%,	MODE(57) =	5.4973%,	MODE(58) =	0.0003%,	MODE(59) =	0.1662%,	MODE(60) =	0.0000%,

FLUTTER MODE TRACKING: 100% = PRIMARY MODE. 0% = NO CONTRIBUTION TO FLUTTER MODE.											
MODE(1) =	0.0000%,	MODE(2) =	0.6003%,	MODE(3) =	0.0001%,	MODE(4) =	44.2676%,	MODE(5) =	0.0006%,
MODE(6) =	0.8974%,	MODE(7) =	0.0009%,	MODE(8) =	13.9995%,	MODE(9) =	19.0704%,	MODE(10) =	57.8243%,
MODE(11) =	0.0055%,	MODE(12) =	0.5247%,	MODE(13) =	0.0000%,	MODE(14) =	9.4488%,	MODE(15) =	0.0001%,
MODE(16) =	0.0001%,	MODE(17) =	2.0266%,	MODE(18) =	0.0028%,	MODE(19) =	10.1764%,	MODE(20) =	0.0044%,
MODE(21) =	2.6336%,	MODE(22) =	0.3962%,	MODE(23) =	0.0000%,	MODE(24) =	0.0096%,	MODE(25) =	100.0000%,
MODE(26) =	0.0000%,	MODE(27) =	0.9773%,	MODE(28) =	0.0004%,	MODE(29) =	0.0999%,	MODE(30) =	0.4246%,
MODE(31) =	0.0000%,	MODE(32) =	0.0000%,	MODE(33) =	0.0062%,	MODE(34) =	0.0000%,	MODE(35) =	0.1671%,
MODE(36) =	0.0002%,	MODE(37) =	0.0975%,	MODE(38) =	0.0000%,	MODE(39) =	0.4547%,	MODE(40) =	0.0001%,
MODE(41) =	4.9210%,	MODE(42) =	0.0000%,	MODE(43) =	0.0916%,	MODE(44) =	0.4200%,	MODE(45) =	0.0000%,
MODE(46) =	0.0577%,	MODE(47) =	0.0000%,	MODE(48) =	0.0000%,	MODE(49) =	0.2620%,	MODE(50) =	0.1303%,
MODE(51) =	0.1879%,	MODE(52) =	0.0001%,	MODE(53) =	0.1728%,	MODE(54) =	0.0002%,	MODE(55) =	0.0546%,
MODE(56) =	0.0001%,	MODE(57) =	0.0824%,	MODE(58) =	0.0000%,	MODE(59) =	0.0260%,	MODE(60) =	0.0000%,

Table 5: *Modal participation factors* of the first 60 structural eigenmodes for the flutter modes 1 and 2 (T-tail flutter modes), ALLEGRA-S, configuration c01, ISA 15°C, H = 5400 [m]

ing eigenmodes represent the features of an instability state. The highly complex eigenmodes describe the phase shifted vibration of the structure and can be displayed graphically only as snapshots. In Fig. 6 the flutter modes of the (minimal) mass configuration c01 and flight altitude H=5400 [m] are presented as structural deformations interpolated on the aerodynamic panel grid. These flutter shapes correspond to the first six flutter cases in Tab. 3. The topological character of the shape is further described in the right column "flutter type". While at moderate flight speeds the (nominal) vacuum mode dominates the aeroelastic eigenmode at higher velocities several structural modes can become almost equally weighted constituents of the flutter mode. As an example see also the modal participation factors of the two "T-tail" modes in Fig. 5.

4 METHOD OF MODAL CORRECTION

The method of modal correction enables an extension of the aeroelastic simulation model and is used to incorporate both the whirl/thrust and the T-tail effects into the equation of motion. In all cases of the added T-tail and engine related terms the dynamical model requires a linearisation prior to the eigenvalue analysis. All the resulting terms then can be formulated as (deformation dependent) first order extensions of the equation of motion. The approach renders an enhancement and extension of the aeroelastic simulation model, whose basic terms were built up by the Finite Element structural part (NASTRAN) and the Doublet Lattice aerodynamic part. Both the incorporation of the extension terms and the solving of the flutter equations still have to be executed within the aeroelastic tool ZAERO. The linear character of the eigenvalue solution algorithm as well as the specific communication features of the aeroelastic tool ZAERO for the integration of additional simulation model components allowed this approach. To incorporate the T-tail and the engine specific terms into the aeroelastic equation of motion of the flying aeroplane the method of modal correction was applied in a similar manner, regardless of the physical origin of the model extensions (gyroscopic mass effects, engine thrust or HTP trim loads).

This approach represents an approximate solution of a system where predominant terms are to be expanded by minor terms of second order magnitude. Under the assumption of small magnitude of the correction terms the uncorrected system will not be affected significantly. Consequently the (here: *real*) structural eigenmodes, which are to be imported into the aeroelastic solver ZAERO, are still valid and represent not only the baseline but — in a

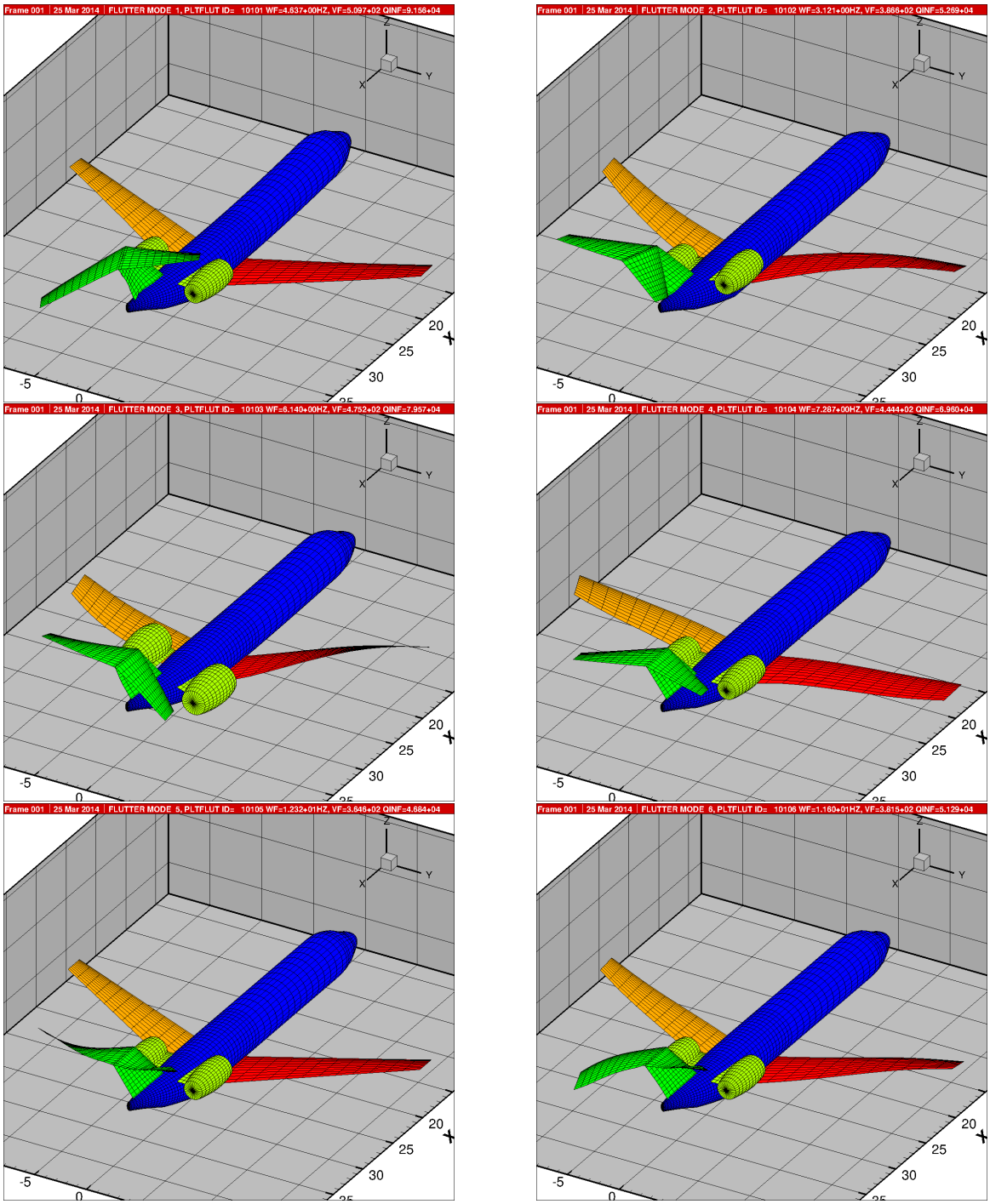

Figure 6: Flutter modes 1 – 6 referring to Tab. 3, ALLEGRA-S, configuration c01, ISA 15°C, H = 5400 [m] (from upper left to lower right); compare Tab. 3

sufficiently high number — also the expanded system.

The modified homogeneous equation of motion in generalised coordinates (designated by an asterix *), where the modal correction — or rather expansion — Δ is now already incorporated, looks like:

$$(M^* + \Delta M^*)\,\ddot{q} + (D^* + \Delta D^*)\,\dot{q} + (K^* + \Delta K^*)\,q = 0 \quad . \tag{1}$$

Here the added correction matrices also have been transferred into the modal space by the modal matrix Φ, where

$$\Delta M^* = \Phi^T \Delta M \Phi \quad , \qquad \Delta D^* = \Phi^T \Delta D \Phi \quad , \qquad \Delta K^* = \Phi^T \Delta K \Phi \quad . \tag{2}$$

The modal matrix Φ contains either the full set of eigenvectors of the eigenvalue solution of the baseline system or only a subspace set, i.e. it must not be quadratic. As a "convergence" criteria it only should be guaranteed that there is a sufficient and suitable quantity of eigenmodes included to be capable of representing the dynamic behaviour also of the new, gyroscopic system (here: 86 structural eigenmodes).

5 EFFECT OF ENGINE THRUST AND ROTOR SPIN

The thrust matrix is deflection proportional and counter acting as an additional, geometric stiffness, whereas the gyroscopic term is velocity proportional, being derived from the Coriolis forces (mass acceleration) which are caused by the motion of the spinning masses within the rotating frame.

The antimetric, but linear gyroscopic matrix contains in general the gyro momenta caused by the engine rotation around both the global x-axis and (optional) other minor terms perpendicular to the major angular momentum which can arise from, for example, transmission components (to be multiplied further by the actual transmission ratios n_i):

$$D_j^{Gyr} := \Omega \begin{bmatrix} 0 & 0 & 0 & 0 & 0 & 0 \\ 0 & 0 & 0 & 0 & 0 & 0 \\ 0 & 0 & 0 & 0 & 0 & 0 \\ 0 & 0 & 0 & 0 & -n_z\Theta_z^j & +n_y\Theta_y^j \\ 0 & 0 & 0 & +n_z\Theta_z^j & 0 & -\Theta_x^j \\ 0 & 0 & 0 & -n_y\Theta_y^j & +\Theta_x^j & 0 \end{bmatrix} \equiv \Delta D_j \quad . \tag{3}$$

This matrix is skew symmetric and energetically conservative, in contrast to the asymmetric and thus non-conservative but also linear thrust term, containing all six possible components of forces and moments arising from the impulse generation of the engines,

$$K_j^{Geo} := \begin{bmatrix} 0 & 0 & 0 & 0 & +F_z^j & -F_y^j \\ 0 & 0 & 0 & -F_z^j & 0 & +F_x^j \\ 0 & 0 & 0 & +F_y^j & -F_x^j & 0 \\ 0 & 0 & 0 & 0 & +M_z^j & -M_y^j \\ 0 & 0 & 0 & -M_z^j & 0 & +M_x^j \\ 0 & 0 & 0 & +M_y^j & -M_x^j & 0 \end{bmatrix} \equiv \Delta K_j \quad , \tag{4}$$

with "j" being the index denominating each of the two engines. The components of these two matrices refer to the six spacial degrees of freedom of the engine reference point (c.g.;

thrust point of application). Especially for the case of one single main engine rotor the matrices get simpler with less component values.

Flutter case No.	Eigen mode No.	Frequency f [Hz]	EAS [m/sec]	TAS [m/sec]	Flutter type
1	5	f = 1.0982 +3.1 [%]	282.6246 −2.0 [%]	518.5342 −2.0 [%]	Wing-sym (vert) (RB)
2	8	f = 4.6312 <0.1 [%]	377.1631 <0.1 [%]	691.9848 <0.1 [%]	T-tail (fuselage-bend)
3	9	f = 3.1408 <0.1 [%]	287.2391 <0.1 [%]	527.0004 <0.1 [%]	T-tail (fuselage-roll)
4	14	f = 6.1033 <0.1 [%]	346.9854 <0.1 [%]	636.6177 <0.1 [%]	Wing-ant (vert) (+Eng)
5	15	f = 7.2954 <0.1 [%]	325.0003 <0.1 [%]	596.2813 <0.1 [%]	Wing-sym (hori)
6	17	f = 8.2723 <0.1 [%]	394.2786 <0.1 [%]	723.3868 <0.1 [%]	Wing-ant (vert)
7	19	f = 11.5748 <0.1 [%]	274.1028 <0.1 [%]	502.8990 <0.1 [%]	HTP-ant
8	20	f = 11.6245 <0.1 [%]	250.1980 <0.1 [%]	459.0407 <0.1 [%]	HTP-sym
9	21	f = 12.7850 <0.1 [%]	275.5964 <0.1 [%]	505.6394 <0.1 [%]	HTP-ant

Table 6: Classification of *flutter modes*, ALLEGRA-S, configuration c01 (43,71 [t]), ISA 15°C, H = 11000 [m] — with engine thrust and gyroscopics; deviation from baseline version

The baseline version of the ALLEGRA-S simulation model had been expanded by the presented additional linear engine related terms which result from the operation of the engines in flight, and then each of them had been compared quantitatively to the results of the baseline configuration. Both the gyroscopic moments and the force vector of the engine thrust are applied to a common grid point (FEM node) in the global coordinate system. All the test cases, i.e. the mass configurations c01 and c09 at the flight altitudes 5400[m] and 11000[m], had been analysed after having been furnished with the thrust and the gyroscopic moments. Representative results are shown in Tab. 6 for the flight altitude 11000 [m] of mass configuration c01. There also the differences from the baseline case are given as the respective percentage values. It can be seen that the results of the flutter analyses with gyroscopic terms in general do not differ substantially from the baseline case without the model extensions and the deviations remain below 0.1 [%]. In order to assess the (low) impact of the added physical phenomena caused by the engines in operation on the stability behaviour of this forward swept aeroplane a look on the engine placement might be helpful. In order not to disturbe the (laminar) wing aerodynamics the engine nacelles are placed in the rear part of the aircraft at both sides of the fuselage. The attachment stiffness between the engine nacelles and the fuselage is necessarily high and hampers the engines in making large relative deflection amplitudes. By this means the engine rotors are disabled from executing significant pitching or yawing rotations and thus contributing

with their own gyroscopic properties to the structural eigenmodes. One exception can be seen in the first flutter case of mass configuration c01 at 11000 [m], which clearly has been affected by the gyroscopic terms. This mode no. 5 is dominated by a rigid body movement plus elastic wing bending and carrying out plunge and pitch deformations. Both the flutter frequency (+3.1 [%]) and the flutter speed (−2.0 [%]) exhibit large relative deviations.

The flutter behaviour of this aircraft is presumably not sensitive due to the specific engine placement at the fusalage. Nevertheless because of the elevated angular momentum of these engines it was considered worthwile to submit the flutter analysis of this configuration (and the respective equations of motion) to a model extension by the engine related terms in focus. Both for the flutter frequencies and for the flutter flight speeds the impact of the rotating engines remains quite moderate, but with different boundary conditions like the attachment stiffness (or a shifted c.g. position) they should not considered to be negligible. To demonstrate the influence a lowered engine attachment stiffness together with the gyroscopic behaviour can exert on the flutter state a case of diminished rotational stiffness, for example as it could be the case due to a partial suspension failure, was simulated (factor $1/25 = 4$ [%]). In Fig. 6 and Tab. 7 the results are shown for four flutter modes of the mass configuration c04. Concerning the flutter frequencies all values are lifted which against the background of additional d.o.f. coupling caused by the gyroscopics and the follower force of the thrust appears resonable. In contrast to the frequencies all flutter flight speeds (critical speeds) here move to lower values. Since a (linear) flutter state is the result of a balance

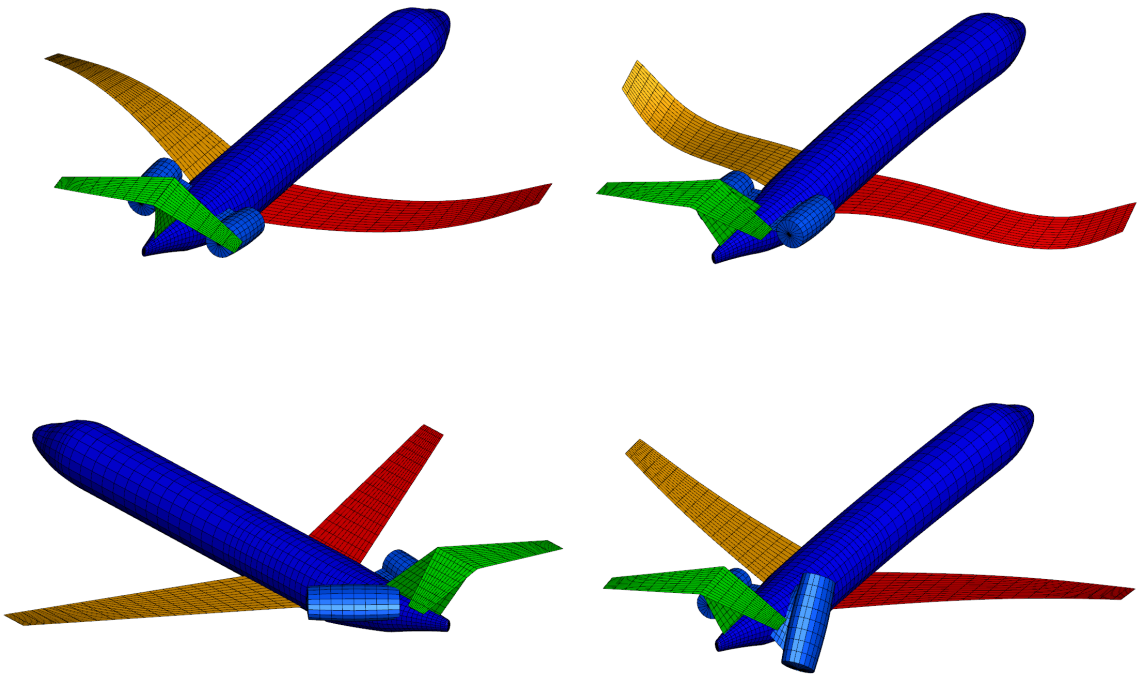

Figure 7: Four *flutter modes* ALLEGRA-S, configuration c04 (M=0.75), ISA 15°C, H = 0 [m] (upper left to lower right) — with engine thrust and gyroscopics and reduced suspension stiffness ($c/c_0 = 4$[%]); compare Tab. 7

between all participating aeroelastic influences (forces), it must be stated that this drift should not be considered to be a general tendency. Instead every aeroplane configuration should be investigated individually whether the engine effects have a stabilizing impact — with their omission one would be on the conservative side —, or would lower the flutter speed thus causing a loss in stability margins.

Flutter case No.	Eigen mode No.	Frequency f [Hz]	EAS [m/sec]	Flutter type
1	4	f =1.9288 +1.02 [%]	292.64 − 0.70 [%]	Wing-ant (vert)
2	7	f =4.5046 +0.32 [%]	395.02 −0.17 [%]	Wing-sym (vert)
3	3	f =1.5753 N/A [%]	88.996 N/A [%]	Engine-whirl (right)
4	5	f =2.5349 N/A [%]	262.72 N/A [%]	Engine-whirl (left)

Table 7: Classification of *flutter modes*, ALLEGRA-S, configuration c04 (M=0.75), ISA 15°C, H = 0 [m] — with engine thrust and gyroscopics and reduced suspension stiffness ($c/c_0 = 4[\%]$); deviation from baseline version; compare Fig. 7

Concerning the eigenmodes there are two flutter modes displayed for the engine baseline configuration plus gyroscopics plus thrust force to exemplify the effect of the engine model extensions visually (see flutter modes 3 and 4 in Fig. 6 and Tab. 7). This demonstration case with a significantly lowered attachment stiffness had been analysed in order to simulate a (partial) failure of the engine suspension. Although their mathematical complexity is difficult to be demonstrated with only one single sketch, two snapshots of the eigenmodes have been chosen where the symmetry breaking character of the gyroscopics is to be recognized clearly. In addition to having a highly complex phase shift in the motion of the mode components (as this is also the case in the baseline configuration) here now the symmetry features have vanished and the two flutter eigenmodes appear totally asymmetric. As already mentioned above the complexity of the aeroelastic balance of the flutter state does not allow the forecast of the flutter speed in an extrapolation sense. Whereas the two flutter modes 3 and 4 occured only by the lowering of the suspension stiffness the flutter modes 1 and 2 present themselves only very underproportionally affected. Both sign and magnitude of the flutter speed deviation should therefore always be determined in an individual and complete aeroelastic analysis.

6 IMPACT OF THE T-TAIL ON THE FLUTTER STATE

Similar to the approach for the incorporation of the gyroscopic engine terms it was tried in the simulation model to capture the influence of the T-tail empennage architecture on the flutter behaviour. The characteristic features of the T-tail impact are based on the aerodynamic loads acting on the HTP. Two specific physical phenomena can be named to have the possibility to affect the flutter state (frequency and flutter speed): First a lowering

of the structural eigen frequencies by a geometric softening of the VTP structure through a negative HTP load and second a coupling of the rolling and the yawing of the T-tail caused by a component coupling of the HTP degrees of freedom. The latter effect could be formulated also for other aerodynamic surfaces (wings) but in case of the T-tail it is in a specific way amplified by the attachment of the HTP plane at the upper end of the elastic structure of the VTP. In such a way the VTP is not only acting as a "soft" suspension boundary condition for the HTP but even as a "moving" one. Looking at a Δy-*strip* "j" of the HTP surface lying in the x-y plane where only a lift force is acting on (potential theory) the following aerodynamic forces can be summerized in the balance sheet:

$$\left\{ \begin{array}{c} \Delta F_x \\ \Delta F_y \\ \Delta F_z \end{array} \right\}^K_j = \frac{\rho}{2}\, v_\infty^2\, c_a(y)\, \Delta y\, l(y) \left[\begin{array}{ccc} 0 & 0 & 0 \\ -1 & 0 & 0 \\ 0 & 0 & 0 \end{array} \right] \left\{ \begin{array}{c} \alpha \\ \beta \\ \gamma \end{array} \right\}_j \tag{5}$$

and

$$\left\{ \begin{array}{c} \Delta F_x \\ \Delta F_y \\ \Delta F_z \end{array} \right\}^D_j = \frac{\rho}{2}\, v_\infty\, c_a(y)\, \Delta y\, l(y) \left[\begin{array}{ccc} 0 & 0 & +1 \\ 0 & 0 & 0 \\ -2 & 0 & 0 \end{array} \right] \left\{ \begin{array}{c} u \\ v \\ w \end{array} \right\}^{\cdot}_j \quad . \tag{6}$$

They are selfinduced by motion and — coming from the reference (trim) state — appear to be additional to the perturbation state of the flutter calculation. To derive the complete expressions finally to be integrated in the equation of motion the following steps have to be considered:

- To expand the equation of motion of the perturbated state around the reference trim state (e.g. stagnation pressure),
- to formulate the equilibrium around the deformed state (e.g. follower forces), and
- to take into account the linear terms which appear to be proportional both to deformation and velocity.

Possible major impacts on the flutter behaviour can be caused by the new yaw and roll component coupling and are to be expected in the antimetric flutter modes dominated by T-tail participation. Finally it follows for all six force components (d.o.f.) of a *structural node* "j":

$$\left\{ \begin{array}{c} \Delta F_x \\ \Delta F_y \\ \Delta F_z \\ \Delta M_\alpha \\ \Delta M_\beta \\ \Delta M_\gamma \end{array} \right\}^K_j = \left[\begin{array}{cccccc} 0 & 0 & 0 & 0 & 0 & 0 \\ 0 & 0 & 0 & -F_z & 0 & 0 \\ 0 & 0 & 0 & +F_y & 0 & 0 \\ 0 & 0 & 0 & 0 & 0 & 0 \\ 0 & 0 & 0 & -M_z & 0 & 0 \\ 0 & 0 & 0 & +M_y & 0 & 0 \end{array} \right]^{Trim}_j \left\{ \begin{array}{c} u \\ v \\ w \\ \alpha \\ \beta \\ \gamma \end{array} \right\}_j \tag{7}$$

and

$$\left\{\begin{array}{c}\Delta F_x\\ \Delta F_y\\ \Delta F_z\\ \Delta M_\alpha\\ \Delta M_\beta\\ \Delta M_\gamma\end{array}\right\}_j^D = \frac{1}{v_\infty}\left[\begin{array}{cccccc}0 & +F_y & +F_z & 0 & 0 & 0\\ -2F_y & 0 & 0 & 0 & 0 & 0\\ -2F_z & 0 & 0 & 0 & 0 & 0\\ 0 & +M_y & +M_z & 0 & 0 & 0\\ -2M_y & 0 & 0 & 0 & 0 & 0\\ -2M_z & 0 & 0 & 0 & 0 & 0\end{array}\right]_j^{Trim} \left\{\begin{array}{c}u\\ v\\ w\\ \alpha\\ \beta\\ \gamma\end{array}\right\}_j^{\cdot} \quad , \tag{8}$$

or

$$\left\{\begin{array}{c}\Delta F_x\\ \Delta F_y\\ \Delta F_z\\ \Delta M_\alpha\\ \Delta M_\beta\\ \Delta M_\gamma\end{array}\right\}_j^D = \frac{ik}{l}\left[\begin{array}{cccccc}0 & +F_y & +F_z & 0 & 0 & 0\\ -2F_y & 0 & 0 & 0 & 0 & 0\\ -2F_z & 0 & 0 & 0 & 0 & 0\\ 0 & +M_y & +M_z & 0 & 0 & 0\\ -2M_y & 0 & 0 & 0 & 0 & 0\\ -2M_z & 0 & 0 & 0 & 0 & 0\end{array}\right]_j^{Trim} \left\{\begin{array}{c}u\\ v\\ w\\ \alpha\\ \beta\\ \gamma\end{array}\right\}_j \quad . \tag{9}$$

For the trim state derived with the potential theory DLM in ZAERO all the moment terms vanish:

$$M_{y|z}^j \equiv 0 \qquad . \tag{10}$$

In ZAERO the unsteady aerodynamic forces in the modal coordinates $A(k)$ are composed by the generalized aerodynamic matrices $Q_{gg}(k)$ and the factors of the dynamic pressures:

$$A(k) = \frac{\rho}{2}\, v_\infty^2\, \Re(Q_{gg}(k)) + i\, \frac{\rho}{2}\, v_\infty\, \Im(Q_{gg}(k)) \qquad . \tag{11}$$

The aerodynamic T-tail corrections are based on the HTP loading of a trim state. To incorporate the above formulated terms into the flutter algorithm of ZAERO a combining with the generalized *aerodynamic* matrices had been considered first in order to cope with the (explicit) dependency of the flight speed $\frac{1}{v_\infty}$ in the velocity term. This turned out to be impossible due to the inconsistecies in the k and $\frac{1}{v_\infty}$ dependency of the generalized aerodynamic forces and the T-tail extensions. Instead in analogy to the gyroscopic terms the T-tail corrections have been incorporated into the equation of motion through the modal correction of the *structural* system matrices. In a strict sense each flutter analysis should require its own preceding trim calculation. To reduce the calculation effort one (in the T-tail sense) unfavourable trim state with the largest negative HTP loads had been chosen and taken as representative also for the flight states at higher flight speeds. (The variation of the angle of attack had not to be taken into account in the flutter analysis.) So the T-tail terms as they were used here are exactly valid only for one single flight state but considered to be suitable in a conservative sense also for flight states at higher velocities.

Out of the group of available mass configurations of the ALLEGRA-S design (see Tab. 8) the most unfavourable one (c07) with the largest negative HTP load (-993.80 [kg]) had been chosen as the reference level flight trim state. For the sake of completeness there is given an overview over the flutter cases also for this mass configuration c07 in Tab. 9. The strongest impact of the T-tail corrections had to be expected on the two T-tail modes 2 and 3, here as the type of fuselage-bending. The pictures of the respective flutter modes are displayed in Fig. 8. The main results of the flutter calculations are given in Tab. 10 for the two T-tail modes and also flutter mode 1, which is a classical antimetric wing bending

mode but with some share of lateral empennage deflection. Shown are the values of the flutter frequencies (Hz) and flutter speeds (EAS) for the modified cases and the deviations from the baseline case as percentage numbers in Tab. 9. The variations comprise the added T-tail corrections, while in an accumulative sense first the direct trim force related terms and in a second run also the geometric stiffness matrix of the VTP had been incorporated into the simulation model. In all flutter calculations the frequencies went up, whereas the flutter speeds were lowered. Because the values of the resulting deviations around 0.1[%] remained very moderate — and for the possibilty of elevated HTP loads in other trim states — the T-tail corrections were multiplied by the factor 10. Now with values around 1.0[%] the differences became clearer. For a better understanding the flutter curves for the baseline case and the case with the enlarged correction terms (Trim+Geo) are compared in Fig. 9. In the circumstance that only the modes with a strong T-tail participation had been affected (the cyan and the red curves) an additional proof for the correctness of the approach can be seen. An explanation for the low impact of the T-tail corrections on the respective flutter modes could be the fact that these are still dominated by the wing and the fuselage bending in their dynamical behaviour and less by the T-tail deformations.

Mass config.	Mass tot. $[kg]$	x-cg $[m]$	Fuel mass $[kg]$ ([%])	Div. q $\left[\frac{N}{m^2 10^4}\right]$		HTP trim load $\left[\frac{N}{g}\right]$	
				M = .8	M = .9	M = .8	M = .9
c01	43712	19.637	0 (0)	4.6752	4.1643	-570.96	-592.12
c02	43712	20.840	0 (0)	4.6767	4.1630	2186.32	2165.83
c03	62962	19.637	12263 (72)	4.5106	4.0123	-822.40	-852.88
c04	62962	20.840	12263 (72)	4.5433	4.0402	3149.11	3119.59
c05	73365	19.637	12263 (72)	4.4842	3.9876	-958.28	-993.80
c06	73365	20.840	12263 (72)	4.5086	4.0086	3669.39	3634.99
c07	73365	19.637	16980 (100)	4.6157	4.1082	-958.28	-993.80
c08	73365	20.840	16980 (100)	4.7069	4.1904	3669.39	3634.99
c09	73365	20.239	16980 (100)	4.6459	4.1346	1357.47	1322.51

Table 8: Definitions of the ALLEGRA-S mass configurations and HTP trim loads (yellow highlighted = the reference trim state)

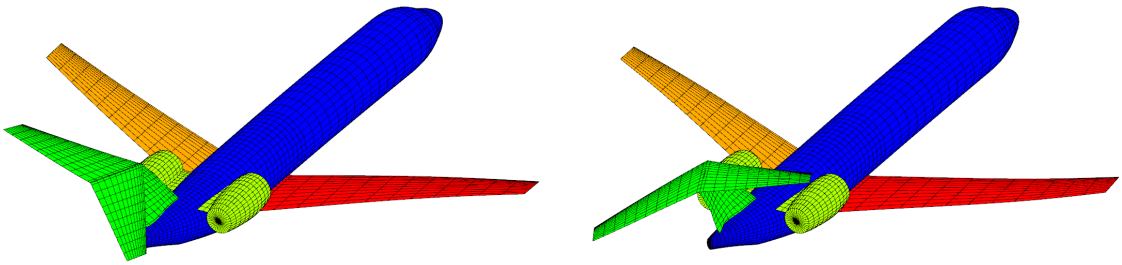

Figure 8: T-tail *flutter modes* 2 and 3 ALLEGRA-S, configuration c07 (M=0.8), ISA 15°C, H = 5400 [m]

Flutter case No.	Eigen mode No.	Frequency f [Hz]	EAS $[m/sec]$	TAS $[m/sec]$	Flutter q $\left[\frac{N}{m^2 10^4}\right]$	Flutter type
1	8	2.1282	300.02	395.54	5.513	Wing-ant (vert)
2	9	4.4051	353.67	466.27	7.661	T-tail (fuselage-bend)
3	10	3.9193	286.23	377.36	5.018	T-tail (fuselage-bend)
4	12	4.4344	384.65	507.11	9.062	Wing-sym (vert)
5	13	5.2561	328.57	433.18	6.612	Wing-sym (hori)
6	18	12.3686	276.45	364.47	4.681	HTP-sym
7	23	11.8417	279.16	368.04	4.773	HTP-ant
8	26	13.0237	275.79	363.60	4.658	HTP-ant

Table 9: Classification of *flutter modes*, ALLEGRA-S, configuration c07 (73,36 [t]), ISA 15°C, H = 5400 [m]

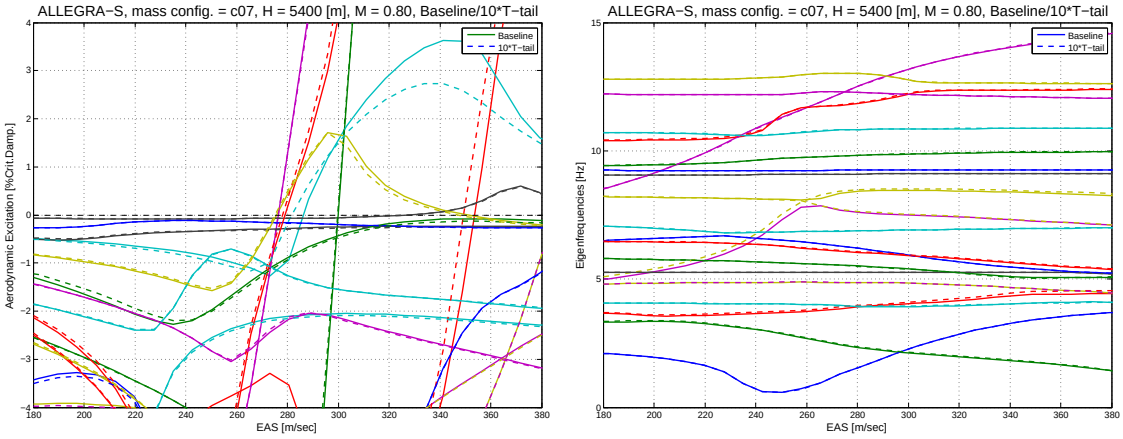

Figure 9: *Aerodynamic excitation* and *frequencies* of the first 26 elastic eigenmodes, ALLEGRA-S, configuration c07, ISA 15°C, H = 5400 [m] (baseline and T-tail corrected)

Case No.	+Trim		+Trim+Geo		+Trim*10		+(Trim+Geo)*10	
	f [Hz]	EAS $\left[\frac{m}{sec}\right]$	f [Hz]	EAS $\left[\frac{m}{sec}\right]$	f [Hz]	EAS $\left[\frac{m}{sec}\right]$	f [Hz]	EAS $\left[\frac{m}{sec}\right]$
1	2.131	299.99	2.130	300.00	2.155	299.72	2.152	299.82
	0.13%	-0.01%	0.12%	-0.01%	1.28%	-0.10%	1.13%	-0.07%
2	4.410	353.40	4.415	353.15	4.458	351.28	4.511	349.44
	0.11%	-0.08%	0.24%	-0.15%	1.20%	-0.68%	2.41%	-1.20%
3	3.920	286.04	3.922	285.74	3.926	284.36	3.943	281.83
	0.02%	-0.07%	0.08%	-0.17%	0.18%	-0.65%	0.61%	-1.54%

Table 10: Flutter results of the corrected *T-tail modes* and deviations form the baseline configuration, ALLEGRA-S, mass configuration c07 (73,36 [t]), ISA 15°C, H = 5400 [m]

7 SUMMARY AND CONCLUSIONS

The objective of this research work are modelling techniques for describing the dynamical behaviour and the struchtural interaction between specific components of the aircraft — like large rotating engine masses, the thrust vector of the engine or the T-tail empennage — and the fuselage of a flying, forward swept wing aircraft. One focus lies on the coupling of the thrust of the deflected engine (as a follower force) with its structural surroundings. The gyroscopic effects arise from the whirl moments formed by the total rotational momentum of the quasi-rigid engine rotors, whereas the T-tail effects basically stem from the static aerodynamic loads acting on the HTP and thus are trim state (and flight condition) dependent. As specific T-tail phenomena, the dynamic pressure effects of the yawing horizontal stabilizer and the geometric softening of the VTP structure by the negative lift forces are included. While the whirl moment of the engine rotor combines the pitch and the yaw degrees of freedom, the T-tail effect couples the yaw and the roll components of the involved d.o.f. All the resulting terms can be formulated as (deformation dependent) first order extensions of the equation of motion. In any case of the added T-tail and engine related terms the dynamical model requires a linearization prior to the eigenvalue analysis. The approach renders an enhancement and extension of the aeroelastic simulation model, which was built up by a Finite Element structural part (NASTRAN) and a Doublet Lattice aerodynamic part. The solving of the flutter equations had been executed within the aeroelastic tool ZAERO. The method of modal correction (or modal extension) is used to incorporate both the whirl/thrust and the T-tail effects into the equation of motion. The linear character of the eigenvalue solution algorithm as well as the specific communication features of the aeroelastic tool ZAERO for the integration of additional simulation model components were successfully used. In order to take into account also the characteristics of the flexible engine-fuselage interface, attachment stiffnesses had been varied.

H	$v_{krit}(c01)$	$v_{krit}(c09)$	$1,15 * v_D$
[m]	[m/sec] EAS (TAS)	[m/sec] EAS (TAS)	[m/sec] EAS (TAS)
5400	276. (364.)	275. (363.)	233. (307.)
11000	250. (459.)	219. (402.)	172. (316.)

Table 11: The critical flight speeds (lowest flutter speeds) of the two ALLEGRA-S mass configurations c01 und c09 in comparison to $1,15 * v_D$

As simulation platform an aeroelastic model of the ALLEGRA-S configuration under several flight conditions had been used for the dynamic analyses. Representing the main research object in this investigation it serves as a demonstrator model and as dynamic reference configuration for both the structural and the aerodynamic calculations. The investigation covered modelling techniques for simulating the dynamics of the structural behaviour of the free flying aircraft in the frequency domain. As results of the flutter analyses the critical velocities and the flutter frequencies of the respective complex flutter eigenmodes are presented (see Tab. 11). Various flutter cases could be distinguished. The impact on the stability behaviour is flutter case dependent but could in general be described as a stiffening effect in the sense of a rising flutter frequency. Although cases of systems becoming more stable by rising of the flutter speed are in general possible here only a (small) destabilizing impact of the model corrections could be observed. In any case a clear distinction between

the symmetric and the antimetric flutter modes was no longer possible since the antimetric components of the gyroscopic and the T-tail matrices cause additional coupling of the degrees of freedom which results in complete asymmetric eigenmodes. The outcome of different parameter studies have been presented as numerical results of non-matched flutter analyses (for constant Ma numbers) as well as the overall dynamical behaviour w.r.t. the change of flight speed have been illustrated in flutter diagrams.

8 COPYRIGHT STATEMENT

References

[1] Scanlan, R.H.; Truman, J.C.: *The gyroscopic effect of a rigid rotating propeller on engine and wing vibration modes.* J. Aero. Sci. 17: 653-9, 667, 1950.

[2] Suciu, Emil: *MSC/NASTRAN flutter analyses of T-tails including horizontal stabilizer static lift effects and T-tail transsonic dip.* MSC/NASTRAN World Users Conference, Newport Beach, Ca., June 3-7, 1996.

[3] Hodges, Dewey H.; Patil, Mayuresh J.; Chae, Seungmook. *Effect of thrust on bending-torsion flutter of wings*: AIAA 2001-1656.

[4] Arizono, H.; Kheirandish, H.R.; Nakamichi, J.: *Flutter simulations of a T-tail configuration using non-linear aerodynamics.* Int. Journal Numer. Meth. in Engng. 2007; 72:1513–1523.

[5] Van Zyl, Louw H.: *A DLM for T-tails.*

[6] Rodden, William P.: *Theoretical and Computational Aeroelasticity.* Crest Publishing, 1^{st} Edition, 2011.

[7] Voss, Ralph, et al.: *DLR Project iGreen, Final report.* DLR, Institut für Aeroelastik, Göttingen, Februar 2012.

[8] Waitz, Stefan: *MBS Analysis of a Free Flying Helicopter with Fully Articulated Rotor.* Proc. European Rotorcraft Forum ERF2014, Southampton, 2014.

[9] Krüger, W. R.; Klimmek, T.; Liepelt, R.; Schmidt, H.; Waitz, St.; Cumnuantip, S.: *Design and aeroelastic assessment of a forward-swept wing aircraft.* CEAS Aeronautical Journal: Volume 5, Issue 4 (2014), Page 419-433, 2014.

[10] Waitz, Stefan; Hennings, Holger: *The aeroelastic impact of engine thrust and gyroscopics on aircraft flutter instabilities.* 16. IFASD, St.Petersburg, 2015.